Materials Transactions, Vol. 57, No. 10 (2016) pp. 1816 to 1822

Formation of Al-Ni Intermetallic Layers Lining Microchannels Produced by Powder-Metallurgical Process Using Aluminum Sacrificial Cores

Tatsuya Ohmi and Naoya Hayashi*

Division of Materials Science, Faculty of Engineering, Hokkaido University, Sapporo 060–8628, Japan

The mechanism of *in-situ* formation of Al-Ni intermetallic lining layers during microchannel formation in nickel bodies by a powder-metallurgical process has been investigated. Aluminum wire was used as a sacrificial core that gives the shape of the microchannel and supplies the alloying element for the lining layer. Nickel powder compacts with 29(±1)% porosity containing aluminum wires were heated from room temperature and then quenched at various temperatures between 873 K and 1473 K. Porous intermetallic lining layers were clearly recognized at temperatures above 1073 K. Each lining layer was built up from an outward-growing layer and an inward-growing layer. Change in the voidage in the outward-growing layer during heat treatment and the formation of a high-voidage zone around the lining layer were accounted for in terms of phase equilibria and unequal diffusion rates of the alloy elements in the Al-Ni intermetallic compounds and nickel solid solution.
[doi:10.2320/matertrans.M2016206]

(Received June 3, 2016; Accepted August 10, 2016; Published September 16, 2016)

Keywords: *microchannel device, microchannel heat exchanger, microreactor, microchannel lining, microporous structure, intermetallic compound, nickel aluminide, powder metallurgy, unequal diffusion rates, Kirkendall voids*

1. Introduction

Development of high-efficiency heat exchangers is one of main issues in a wide range of technological fields including industrial waste heat recovery and thermal management of high-power microelectronic devices. In recent years, microchannel devices such as microreactors[1–13] and microchannel heat sinks[14–18] have actively been investigated with attention on the excellent heat exchange capability coming from the high surface to volume ratio of the microchannel structure. The heat exchange capability is one of the essential properties in the microreactor systems for precise control of reaction temperatures and effective use of heat from external sources. Metallic microchannel devices particularly provide superior heat transfer performance by combining the microchannel structure and the material with good heat conductivity. In addition, the metallic materials are better adapted to high-temperature applications because of their good heat resistance and ease of property control by means of alloying.

Several powder-metallurgical processes have been investigated to produce microchannels directly in metal bodies with simple operations.[19–25] The space-holder method[19–21] using evaporative or soluble patterns of microchannel space (so-called space-holders) produces microchannels in sintered metals. Resins were considered to be used for the evaporative space-holders which were removed by heating during the sintering process.[19] Metallic space-holders soluble in a dilute acid or alkaline solution were also examined: they were removed chemically or electrochemically at room temperature before or after the sintering process.[20,21]

The sacrificial-core method[22–25] also uses metallic patterns of microchannel space. However, the metallic patterns in this method are not removed but used as the source of the alloying element(s) of lining layers surrounding the microchannels, and thus they are called sacrificial cores. Figure 1 illustrates the concept of this method. The metal to compose the device body, the body metal, has higher melting point than that making up the sacrificial core, the sacrificial-core metal. A body-metal powder compact containing a sacrificial core is sintered at temperatures between the melting points of these metals. During sintering, molten sacrificial-core metal migrates to the body-metal powder region by infiltration and/or diffusion to produce a microchannel and an alloy lining layer simultaneously. The formation behaviors of the microchannel and also the structure and composition of the lining layer would vary according to the combination of the body metal and the sacrificial-core metal as well as the process conditions of powder compaction and sintering. If the lining layers acquire various functions through this process and additional simple post processes as appropriate, low-cost production of high-performance microchannel devices becomes reality.

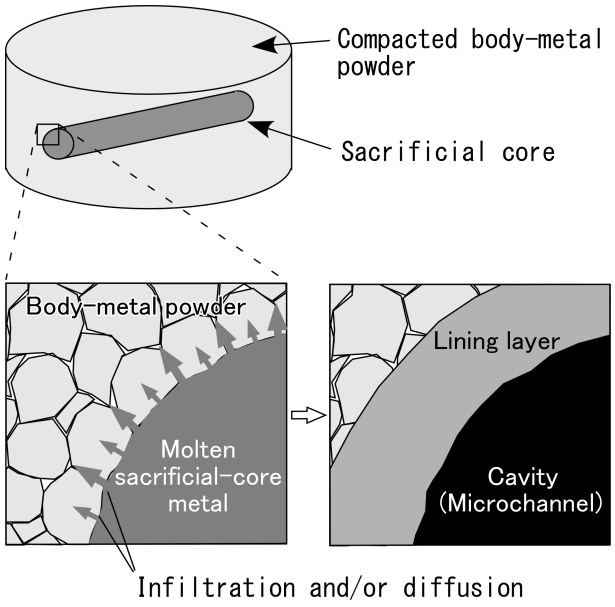

Fig. 1 Schematic representation of the concept of the sacrificial-core method.

*Graduate Student, Hokkaido University. Present address: Nippon Steel & Sumikin Research Institute Corporation, Tokyo 100–0005, Japan

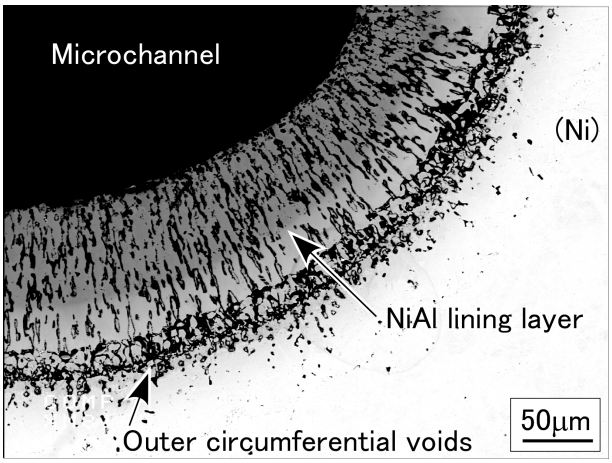

Fig. 2 Typical structure of the Al-Ni intermetallic lining layer produced from nickel (body metal) powder and aluminum (sacrificial-core metal) wire (d = 500 μm).[25)]

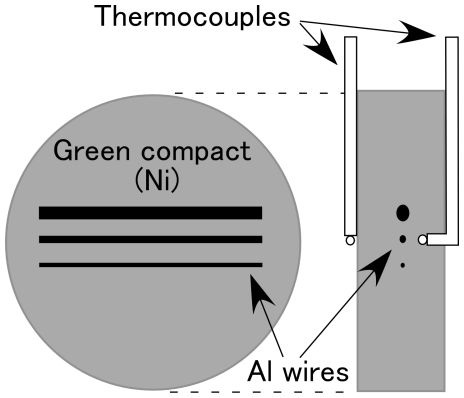

Fig. 3 Schema of the green compact and the thermocouple setup.

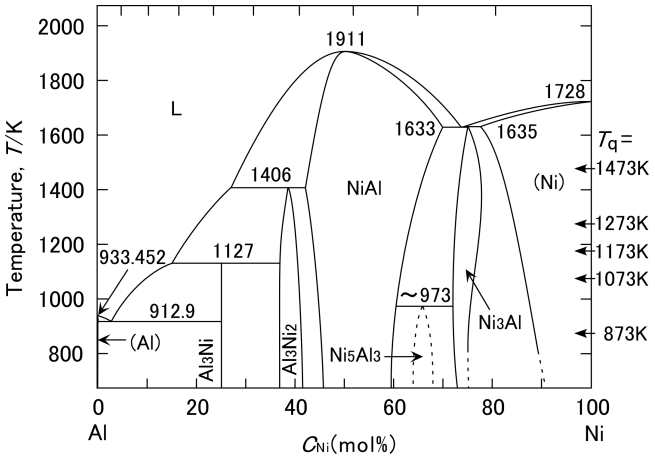

Fig. 4 Al-Ni binary alloy phase diagram based on the report by Okamoto[27)] and the quenching temperatures (T_q).

Figure 2 shows a typical structure of the lining layer produced by the sacrificial-core method with a combination of nickel (body metal) and aluminum (sacrificial-core metal)[25)]. The lining layer mainly consists of NiAl and has peculiar porous structure in which long and thin micropores have grown along the thickness direction of the lining layer.[25)] Such a porous structure of the inner wall of the microchannel is expected to improve flow boiling stability and enhance forced convective heat transfer[16–18)]. In addition, the NiAl intermetallic compound has a high thermal conductivity, good heat resistance and excellent corrosion resistance.[26)] On the other hand, many fine voids are observed near the boundary between the lining layer and the sintered body-metal region. These outer circumferential voids are considered undesirable for the heat transfer performance of the microchannel devices. However, the guidelines for controlling such structures have not been established because the formation mechanism of the Al-Ni intermetallic lining layer is still unclear. In the present study, therefore, we investigated the formation process of the Al-Ni intermetallic lining layer during sintering, especially focusing on the changes in its growing rate, constituting phase(s) and porous structure.

2. Experimental Procedure

In order to investigate the structure change of the lining layer during sintering, we conducted quenching experiments using nickel powder compacts containing aluminum sacrificial cores. The average diameter of the nickel powder particles was 5 μm. The shape of the sacrificial core was a straight wire 10 mm in length and 100, 200 or 500 μm in diameter (d). In the present paper, results of the 500 μm-diameter sacrificial core are examined. Those of the other sacrificial cores will be referred to in the future papers. The purity of the nickel powder was 99.8 mass%, and that of the aluminum wire was 99.98 mass%. Thirteen grams of nickel powder and three aluminum sacrificial cores with different diameters were cold-pressed into a cylindrical green compact in a metal mold using a unidirectional pressure of 460 MPa. The resulted green compact had a diameter of 20 mm and nominal height of 5 mm, and its porosity, E, was 29(±1)%. This green compact porosity was chosen to provide the lining layer of high voidage[25)]. Figure 3 schematically depicts the green compact and the setup of thermocouples. The initial cross-sectional shape of each aluminum wire was round. However, the sacrificial cores were distorted into an oblate figure by unidirectional pressing, and the resulted microchannels and lining layers often inherited the deformation as seen in Fig. 2. The green compact specimen was heated in an argon atmosphere at a constant rate (R_h) of 0.2 Ks^{-1} from room temperature to a given quenching temperature, T_q, and then immersed in a Woods metal bath. Figure 4 depicts an Al-Ni binary alloy phase diagram[27)] and the quenching temperatures. The constituent phases of the lining layer in each specimen were identified based on the results of concentration analysis by EPMA and the composition ranges of the equilibrium phases at each T_q.

We also performed metallographic examinations of the furnace-cooled specimens with various green compact porosities from the experiments described in the previous paper[25)].

3. Results and Discussion

3.1 Structure evolution around the microchannel

Figure 5 presents back-scattered electron images of the

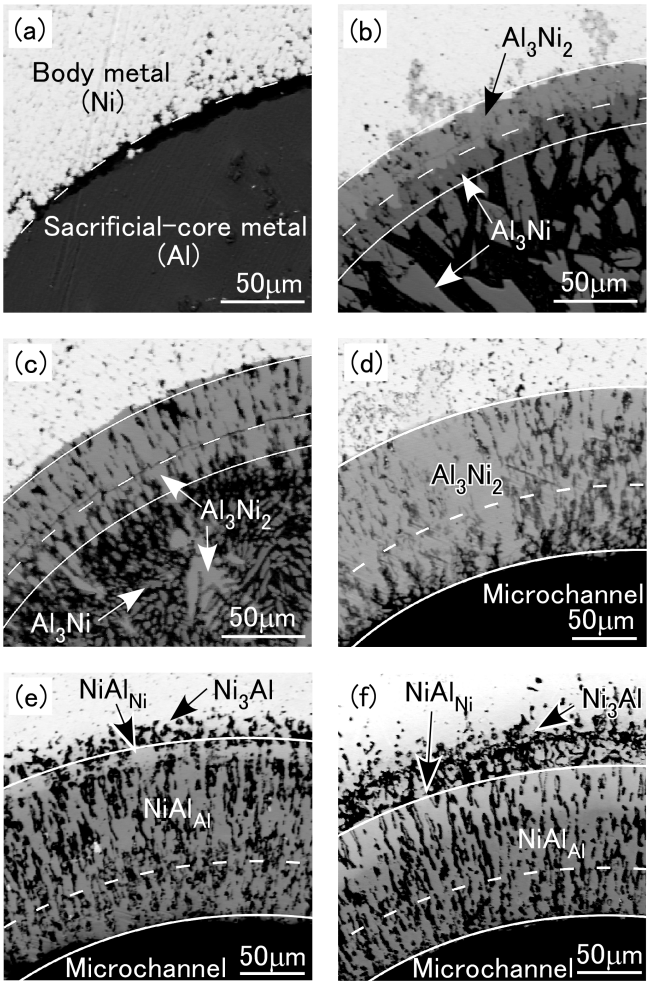

Fig. 5 Structures near the outer periphery of the former sacrificial-core region in the specimens quenched from 873 K (a), 1073 K (b), 1173 K (c), 1273 K (d), 1473 K (e), and furnace-cooled from 1473 K (f). Dashed line: Outer periphery of the sacrificial core before melting. Solid lines: Outer and inner peripheries of the lining layer. $E = 29(\pm1)\%$ and $d = 500$ μm.

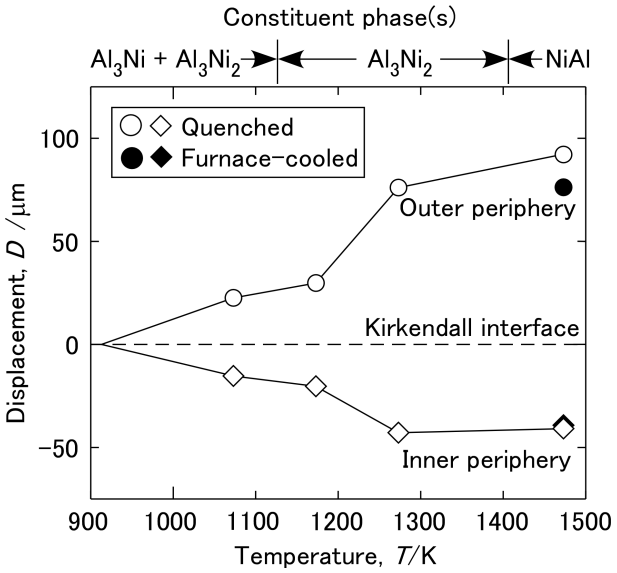

Fig. 6 Growth behavior of the lining layer obtained from the results presented in Fig. 5.

structures near the outer periphery of the former sacrificial-core region in the quenched specimens 29(±1)% in green compact porosity. The solid lines on each photograph are the approximate ellipses of the outer and inner peripheries of the lining layer; the dashed line is the ellipse fitted to the outer periphery of the sacrificial core before melting and superimposed concentrically. As shown in Fig. 5(b), the lining layer grew both outward and inward from the initial boundary between the sacrificial core and the body-metal region. The constituent phases of the outward-growing layer and the inward-growing layer at 1073 K were Al_3Ni_2 and Al_3Ni, respectively. The Al_3Ni phase is in equilibrium with the Al-rich liquid in the temperature range of 912.9–1127 K according to the phase diagram in Fig. 4. The Al_3Ni_2 phase was reported as the dominant reaction phase between Al and Ni in the diffusion experiments at various temperatures, e.g., 773 K[28] and 973–1373 K[29]. In the specimen quenched at 1173 K in Fig. 5(c), the constituent phase of the inward-growing layer had changed to Al_3Ni_2 which was in equilibrium with the Al-rich liquid from 1127 to 1406 K. It is noteworthy that the primary intermetallic phase in the resolidified sacrificial-core region is identical with the constituent phase of the inward-growing layer in each of Figs. 5(b) and 5(c). This result indicates that the molten sacrificial core in each specimen contained a considerable amount of nickel just before quenching. The above results suggest that the inward-growing layer was formed by quasi-isothermal solidification by diffusion of nickel into the molten sacrificial core under the slow temperature elevation of 0.2 Ks^{-1}.

Among the series of the quenched specimens depicted in Fig. 5, the microchannel was first observed in the specimen quenched at 1273 K in Fig. 5(d). This indicates that the microchannel had formed in the course of the growth of the lining layer as the Al_3Ni_2 phase. In the specimen quenched at 1473 K in Fig. 5(e), the constituent phase of the lining layer had changed to Al-rich NiAl ($NiAl_{Al}$), and a Ni-rich NiAl ($NiAl_{Ni}$) layer and the outer circumferential voids began to grow near the outer periphery of the lining layer. In addition, a thin Ni_3Al layer was detected on the outer side of the periphery of the outer circumferential void zone. In the furnace-cooled specimen in Fig. 5(f), many voids are distributed in the outer side of the Ni_3Al layer as well as in the inner side. For the constitution of the NiAl layer, it should be noted that the layer often separates into the $NiAl_{Al}$ and $NiAl_{Ni}$ sublayers. Such a pseudo phase separation is caused by a non-proportional composition dependence of the diffusion coefficient in the NiAl phase.[25]

3.2 Growth behavior of the lining layer

Figure 6 quantitatively indicates the growth behavior of the lining layer obtained from the specimens presented in Fig. 5. The vertical axis of the graph indicates the displacement of the inner or outer periphery of the lining layer from the Kirkendall interface i.e., the initial boundary between the sacrificial core and the body-metal region. The displacement was calculated by subtracting the mean radius of the approximate ellipse of the Kirkendall interface from that of the outer (or inner) periphery of the lining layer. The horizontal axis of the graph indicates the quenching temperatures for the quenched specimens and the top temperature for the furnace-cooled

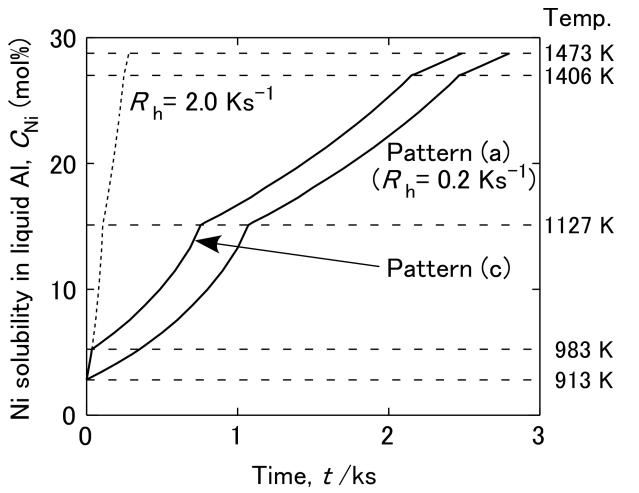

Fig. 7 Temporal changes in nickel solubility in the Al-rich liquid during sintering with various heating patterns. Pattern (a): Constant heating rate of 0.2 Ks^{-1} from room temperature to 1473 K.[23] Pattern (c): Rapid heating at 2 Ks^{-1} from room temperature to 983 K and slow heating of 0.2 Ks^{-1} from 983 K to 1473 K.[23]

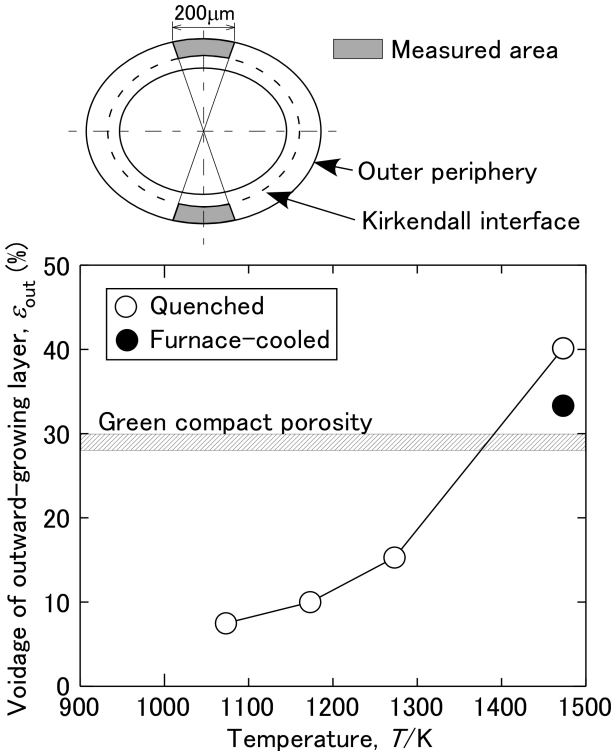

Fig. 8 Change in voidage of the outward-growing layer with temperature elevation during sintering.

specimen. The temperature range of the phases constituting the lining layers are also shown in the graph, which was based on the structure observation in Fig. 5 and the phase diagram in Fig. 4. As Fig. 6 shows, the growth rate of the outward-growing layer drastically increased after the lining layer had become almost single phase of Al_3Ni_2, and it decreased after the microchannel had completed at about 1273 K. It is well known that the diffusion rate of aluminum is higher than nickel in the Al-rich Al-Ni intermetallic compounds i.e., Al_3Ni, Al_3Ni_2, $NiAl_{Al}$.[30–32] Especially in Al_3Ni and Al_3Ni_2, aluminum atoms dominate the diffusion process.[31] In addition, the fact that Al_3Ni_2 is the dominant reaction phase between Al and Ni in its thermodynamically stable temperature range indicates that the diffusion rate in Al_3Ni_2 is higher than any of the other Al-Ni intermetallic compounds. The formation of the microchannel can thus be attributed to the rapid outward diffusion of aluminum through the Al_3Ni_2 single phase lining layer.

However, the inward growth of the lining layer can not be negligible as seen in Fig. 6. It will be a critical problem particularly for the case of much thinner sacrificial cores. Ohmi *et al.*[23] reported that a thick intermetallic layer obstructed the microchannel when formed from a thin aluminum wire (50 μm in diameter) in a nickel (or iron) specimen sintered at a constant heating rate of 0.2 Ks^{-1} from room temperature to 1473 K (Pattern (a), the same heating condition as the furnace-cooling experiments[25]). They also showed that open microchannels were produced when another heating pattern was employed: rapid heating at 2 Ks^{-1} from room temperature to 983 K and slow heating of 0.2 Ks^{-1} from 983 K to 1473 K (Pattern (c)).[23] For their results, one possible explanation can be given from the above concept of quasi-isothermal solidification. Figure 7 illustrates changes with time in nickel solubility in the Al-rich liquid during sintering with various heating patterns, which were calculated using the liquidus line data acquired from the Al-Ni phase diagram. As presented in Fig. 7, a higher heating rate leads to a more rapid increase in nickel solubility. In the molten sacrificial core, quasi-isothermal solidification proceeds when the increase of nickel concentration by diffusion overtakes that of the nickel solubility with the temperature elevation. Therefore, inward growth of the intermetallic layer can be suppressed by adequately rapid heating.

3.3 Void formation during sintering

Figure 8 depicts the change in voidage of the outward-growing layer with temperature elevation during sintering. The measured areas denoted in Fig. 8 correspond to the regions directly subjected to the pressure in the process of powder compaction and less affected by the localized reactive infiltration of molten sacrificial core into the body-metal region[25] than the other regions. According to the results, the voidage is lower than the green compact porosity in the early stages of sintering. It begins to increase after the microchannel formation and exceeds the green compact porosity before the temperature reaches 1473 K. Finally, it slightly decreases during furnace cooling.

Figure 9 schematically illustrates the temporal sequence of diffusion and phase transformation in the lining layer during sintering, which was inferred from the above experimental findings and previous diffusion studies[33–35]. As shown in Fig. 9(a), the rate of aluminum diffusion from the molten sacrificial core to the outward-growing layer in the early stage is higher than that of nickel diffusion in the opposite direction. The lower voidage of the outward-growing layer in the early stage can be explained by such unequal diffusion rates. In Fig. 9(b) which demonstrates the stage after the decomposition of Al_3Ni to Al_3Ni_2 and Al-rich liquid at 1127 K and the subsequent microchannel formation, the dominant diffusion of aluminum from the lining layer to the body-metal region

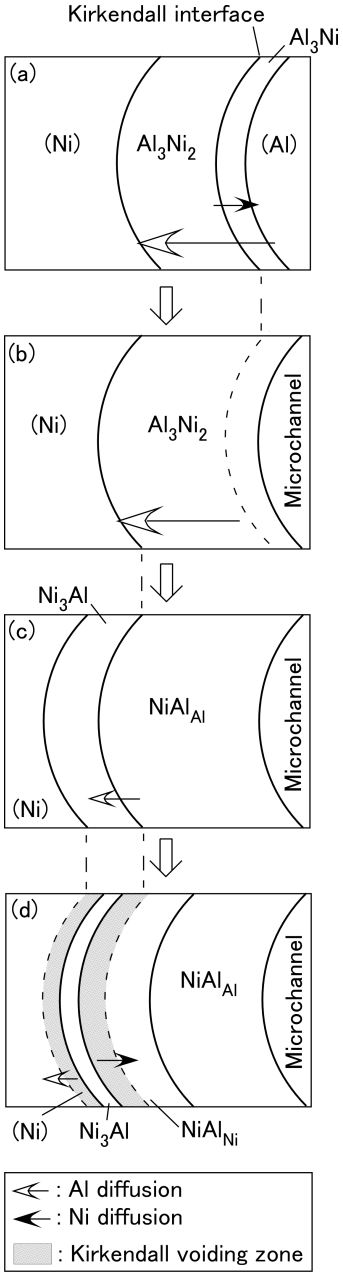

Fig. 9 Temporal sequence of diffusion and phase transformation in the lining layer during sintering. (a) Early stage, (b) Stage after the decomposition of Al_3Ni to Al_3Ni_2 and Al-rich liquid at 1127 K and the subsequent microchannel formation, (c) Stage after the decomposition of Al_3Ni_2 to $NiAl_{Al}$ and Al-rich liquid at 1406 K, (d) Final stage of the structure evolution in the furnace-cooled specimen.

leads to the drastic increase in voidage of the lining layer. Figure 9(c) corresponds to the stage after the decomposition of Al_3Ni_2 to $NiAl_{Al}$ and Al-rich liquid at 1406 K. According to the results of $Ni/NiAl_{Al}$ diffusion-couple experiments[35], a Ni_3Al layer grows from the initial interface towards the Ni region at 1373 K or higher. The aluminum source for the Ni_3Al formation is the $NiAl_{Al}$ phase. The progress of aluminum diffusion decreases the aluminum concentration of the $NiAl_{Al}$ region, and eventually a $NiAl_{Ni}$ layer, which is to be the $NiAl_{Ni}$ sublayer, begins to form at the $Ni_3Al/NiAl_{Al}$ interface towards the $NiAl_{Al}$ region. Figure 9(d) presents the final stage of the structure evolution in the furnace-cooled specimen based on the results of $Ni_3Al/NiAl_{Ni}$ and Ni/Ni_3Al diffusion-couple experiments[33,34]. In the $Ni_3Al/NiAl_{Ni}$ diffusion couple, a $NiAl_{Ni}$ layer grows towards the Ni_3Al region.[34] This can be attributed to the dominant nickel diffusion from Ni_3Al towards the $NiAl_{Ni}$ region. In addition, such an uneven diffusion of nickel and aluminum can produce Kirkendall voids in the new $NiAl_{Ni}$ layer. In the Ni/Ni_3Al diffusion couple, on the other hand, a layer of nickel solid solution grows towards the Ni_3Al region.[33] Watanabe *et al.*[33] described that Kirkendall voids were visible exclusively in the new nickel solid solution layer. They also pointed out that their result indicated that aluminum diffusion was faster than nickel diffusion in the disordered nickel solid solution.[33]

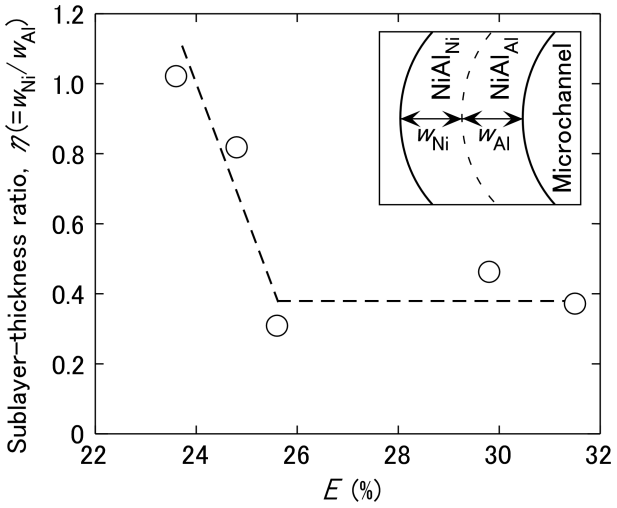

Fig. 10 Relationship between the sublayer-thickness ratio, η, and the green compact porosity, E, in the furnace-cooled specimens. $\eta = w_{Ni}/w_{Al}$, where w_{Ni} and w_{Al} are the average widths of the $NiAl_{Ni}$ and $NiAl_{Al}$ sublayers, respectively.

It is to be noted that the outer periphery of the lining layer was set at the boundary between the NiAl ($NiAl_{Ni}$ + $NiAl_{Al}$) layer and the circumferential high-voidage zone as depicted in Figs. 5(e) and 5(f). Therefore, the influx of nickel atoms into the inner $NiAl_{Ni}$ region in Fig. 9(d), which corresponds to the $NiAl_{Ni}$ sublayer, can decrease the voidage of the region and thus that of the outward-growing layer. This corollary prediction is consistent with the result in Fig. 8. Furthermore, the inward influx of nickel atoms can extend the $NiAl_{Ni}$ sublayer towards the $NiAl_{Al}$ sublayer as illustrated in Fig. 9(d).

3.4 Influence of the green compact porosity on the structures of the lining layer and the circumferential high-voidage zone

The above unsteady topical diffusion in the lining layer is eventually to shift to a quasi-steady state diffusion, in which one-way outward diffusion of aluminum and inward diffusion of nickel promote the growth of the $NiAl_{Ni}$ sublayer. Figure 10 presents the relationship between the sublayer-thickness ratio, η (= w_{Ni}/w_{Al}, where w_{Ni} and w_{Al} are the average widths of the $NiAl_{Ni}$ and $NiAl_{Al}$ sublayers, respectively), and the green compact porosity, E, obtained by the furnace-cooling experiments[25]. According to this result, η has a positive correlation with E when E is below a certain critical level of about 26%, and becomes almost constant when E is over the critical level. This tendency can be explained as follows.

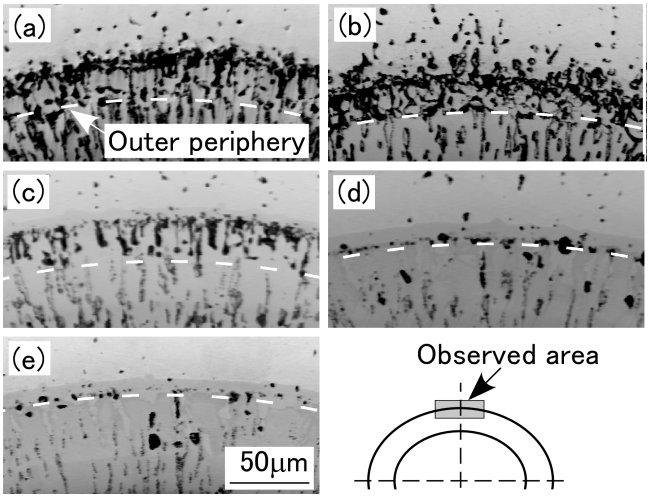

Fig. 11 Structure of the circumferential high-voidage zone in the furnace-cooled specimens with various green compact porosities, 31.5% (a), 29.8% (b), 25.6% (c), 24.8% (d) and 23.6% (e). Dashed line: Outer periphery of the lining layer.

Figure 11 compares the structure of the circumferential high-voidage zone in the furnace-cooled specimens with various green compact porosities. As seen in this figure, a high green compact porosity leaded to formation of a great amount of voids in this zone. The high-voidage zone which prominently developed like that in Fig. 11(a) or (b) must have blocked the diffusion of nickel from the body-metal region to the NiAl lining layer, and thus the growth of the $NiAl_{Ni}$ sublayer. When the diffusion pathway had been kept because of a low initial porosity, in contrast, the supply of nickel atoms must have enabled the continuing growth of the $NiAl_{Ni}$ sublayer, and probably contracted the high-voidage zone as that in Fig. 11(d) or (e).

The results in Fig. 11 indicate the possibility of suppressing the development of the circumferential high-voidage zone by selecting the appropriate powder compacting conditions, but not the methods to control it independently of the voidage of the lining layer which varies depending on the green compact porosity[25]. The formation mechanism of the circumferential high-voidage zone presented in Fig. 9 will, however, provide a useful clue about an effective heat treating schedule during sintering. A detailed study for this subject is the issue in the future.

4. Conclusions

We investigated the formation mechanism of Al-Ni intermetallic lining layers surrounding the microchannels produced by the sacrificial-core method using nickel (body metal) powder and aluminum (sacrificial-core metal) wire 500 μm in diameter. The metallographic analysis of the quenched or furnace-cooled specimens and consideration of previously reported knowledge from various diffusion couple studies provided the following findings.

(1) The lining layer is built up from an outward-growing layer and an inward-growing layer, which are formed by different mechanisms: the former by quasi-isothermal solidification of intermetallic compounds into the molten sacrificial core region, and the latter by reactive diffusion of aluminum into the nickel powder region.

(2) The changes in the major constituting phase and the voidage in the outward-growing layer can be accounted for in terms of phase equilibria and unequal diffusion rates of aluminum and nickel in the Al-Ni intermetallic compounds.

(3) A high heating rate leads to a rapid increase in nickel solubility in the molten sacrificial core, and thus suppresses the inward growth of the intermetallic layer which is to obstruct the microchannel in the case of the small-diameter sacrificial core.

(4) The origin of the circumferential high-voidage zone is the Ni_3Al region temporarily formed in the outer side of the NiAl lining layer; Kirkendall voiding occurred in this region.

(5) A high green compact porosity leads to formation of a great amount of voids in the circumferential high-voidage zone. The high-voidage zone prominently developed is to block the diffusion of nickel from the body-metal region to the NiAl lining layer, and thus the further growth of the $NiAl_{Ni}$ sublayer.

Acknowledgement

This work was partly supported by a grant from the JFE 21 Century Foundation and KAKENHI (C) (19560740).

REFERENCES

1) E.V. Rebrov, G.B.F. Seijger, H.P.A. Calis, M.H.J.M. de Croon, C.M. van den Bleek and J.C. Schouten: Appl. Catal. A Gen. **206** (2001) 125–143.
2) E.V. Rebrov, M.H.J.M. de Croon and J.C. Schouten: Catal. Today **69** (2001) 183–192.
3) G. Kolb and V. Hessel: Chem. Eng. J. **98** (2004) 1–38.
4) P. Pfeifer, K. Schubert, M.A. Liauw and G. Emig: Appl. Catal. A Gen. **270** (2004) 165–175.
5) I. Aartun, T. Gjervan, H. Venvik, O. Görke, P. Pfeifer, M. Fathi, A. Holmen and K. Schubert: Chem. Eng. J. **101** (2004) 93–99.
6) G. Chen, Q. Yuan, H. Li and S. Li: Chem. Eng. J. **101** (2004) 101–106.
7) L. Kiwi-Minsker and A. Renken: Catal. Today **110** (2005) 2–14.
8) I. Aartun, B. Silberova, H. Venvik, P. Pfeifer, O. Görke, K. Schubert and A. Holmen: Catal. Today **105** (2005) 469–478.
9) G.-G. Park, S.-D. Yim, Y.-G. Yoon, W.-Y. Lee, C.-S. Kim, D.-J. Seo and K. Eguchi: J. Power Sources **145** (2005) 702–706.
10) X. Yu, S.-T. Tu, Z. Wang and Y. Qi: Chem. Eng. J. **116** (2006) 123–132.
11) W. Cai, F. Wang, A. van Veen, C. Descorme, Y. Schuurman, W. Shen and C. Mirodatos: Int. J. Hydrogen Energ. **35** (2010) 1152–1159.
12) K.-S. Lin, C.-Y. Pan, S. Chowdhury, W. Lu and C.-T. Yeh: Thin Solid Films **519** (2011) 4681–4686.
13) N.R. Peela and D. Kunzru: Int. J. Hydrogen Energ. **36** (2011) 3384–3396.
14) Richard J. Phillips: *Advances in Thermal Modeling of Electric Components and Systems* Vol. 2, ed. by A. Bar-Cohen and A. D. Kraus (ASME, New York, 1990) pp. 109–184.
15) I. Papautsky, A. B. Frazier and H. Swerdlow: Proc. MEMS'97 (IEEE, 1997) pp. 317–322.
16) D. Deng, Y. Tang, D. Liang, H. He and S. Yang: Int. J. Heat Mass Transfer **70** (2014) 463–477.
17) P.-f. Bai, Z.-c. Yi, B. Tang and G.-f. Zhou: Trans. Nonferrous Met. Soc. China **24** (2014) 900–906.
18) D. Deng, R. Chen, Y. Tang, L. Lu, T. Zeng and W. Wan: Int. J. Multiph. Flow **72** (2015) 275–287.
19) M. Hakamada, Y. Asao, T. Kuromura, Y. Chen, H. Kusuda and M. Mabuchi: Scr. Mater. **56** (2007) 781–783.
20) A.J. Neurohr and D.C. Dunand: Acta Biomater. **7** (2011) 1862–1872.
21) A.J. Neurohr and D.C. Dunand: Acta Mater. **59** (2011) 4616–4630.

22) T. Kimura and H. Hamamoto: Int. J. Powder Metallurgy **10** (1974) 105–108.
23) T. Ohmi, K. Matsuura and M. Kudoh: Int. J. Self-Propagating High-Temperature Synthesis **13** (2004) 121–129.
24) T. Ohmi, M. Sakurai, K. Matsuura, M. Kudoh and M. Iguchi: Int. J. Transport Phenomena **9** (2007) 105–111.
25) T. Ohmi, N. Hayashi and M. Iguchi: Mater. Trans. **49** (2008) 2723–2727.
26) R. Darolia: JOM **43** (1991) 44–49.
27) H. Okamoto: J. Phase Equilib. **14** (1993) 257–259.
28) L. Farber, I. Gotman and E.Y. Gutmanas: Defect and Diffusion Forum **143–147** (1997) 643–648.
29) A. Hibino: J. Jpn. Inst. Metals **57** (1993) 767–773.
30) M.M.P. Janssen and G.D. Rieck: Trans. Metall. AIME **239** (1967) 1372–1385.
31) J.C. Liu, J.W. Mayer and J.C. Barbour: J. Appl. Phys. **64** (1988) 656–662.
32) A. Paul, A.A. Kodentsov and F.J.J. van Loo: J. Alloy. Compd. **403** (2005) 147–153.
33) M. Watanabe, Z. Horita, D.J. Smith and M.C. McCartney: Acta Metall. Mater. **143–147** (1997) 637–642.
34) M. Watanabe, Z. Horita and M. Nemoto: Defect and Diffusion Forum **143–147** (1997) 345–350.
35) M. Watanabe, Z. Horita and M. Nemoto: Defect and Diffusion Forum **143–147** (1997) 637–642.